

Topological Order in an Entangled $SU(2)\otimes XY$ Spin-Orbital Ring

Wojciech Brzezicki,¹ Jacek Dziarmaga,¹ and Andrzej M. Oleś^{1,2}

¹*Marian Smoluchowski Institute of Physics, Jagellonian University, Reymonta 4, PL-30059 Kraków, Poland*

²*Max-Planck-Institut für Festkörperforschung, Heisenbergstrasse 1, D-70569 Stuttgart, Germany*

(Dated: June 25, 2018)

We present rigorous topological order which emerges in a one-dimensional spin-orbital model due to the ring topology. Although an exact solution of a spin-orbital ring with $SU(2)$ spin and XY orbital interactions separates spins from orbitals by means of a unitary transformation, the spins are not independent when the ring is closed, but form two half-rings carrying opposite pseudomomenta. We show that an inverse transformation back to the physical degrees of freedom entangles the spin half-rings with the orbitals once again. This surprising correlation arises on changing the topology from an open to a closed chain, which reduces the degeneracy of the ground-state manifold, leaving in it only the states in which pseudomomenta compensate each other.

PACS numbers: 75.25.Dk, 03.65.Ud, 03.67.Lx, 75.10.Kt

Spin-orbital physics is one of the foundation stones in the theory of frustrated magnetism [1–5]. When degenerate $3d$ orbitals in a transition-metal oxide are partly filled, electrons localize due to large on-site Coulomb interaction and superexchange between magnetic ions includes both spin and orbital degrees of freedom that are strongly interrelated [6]. The orbital degeneracy leads in many cases to a dramatic increase of quantum fluctuation [7], which may trigger exotic order [8] or may stabilize a spin-liquid [9, 10] when different states compete near a quantum critical point. While spin-orbital separation is possible in one-dimensional (1D) systems [11], as observed recently in Sr_2CuO_3 [12], spins and orbitals are usually entangled strongly, as in the archetypal Kugel-Khomskii model [13]. In the $S = 1/2$ $SU(2)\otimes SU(2)$ chain [14, 15], both ground state [16] and excited states [17] are entangled, similar to the $S = 1$ $SU(2)\otimes SU(2)$ chain which plays a prominent role in perovskite vanadates [3–5, 18]. Only in exceptional cases can such 1D models be solved exactly, for example at the $SU(4)$ point [19] or for a valence-bond state [20] of alternating spin and orbital singlets [21], but even in these situations the spins and orbitals cannot be separated from each other.

In real materials the symmetry between spin and orbital interactions is absent. Orbital interactions generically have lower symmetry than spin ones [22], being usually Ising- or XY -like [23]. The XY case is quantum and in general the orbitals cannot be separated from the spins [24]. In this context the 1D spin-orbital $SU(2)\otimes XY$ model introduced by Kumar [25] is surprising — by a change of basis, the $S = 1/2$ spins decouple from the orbitals in an *open* chain. The orbital interactions remain formally unchanged but the spin ones are gauged away. The spins then appear free and the ground state has large degeneracy (2^L for chain length L) [25].

Frustrated spin systems are at the forefront of modern condensed matter theory and experiment [26–28], in large part for the investigation of topology in many-body physics. A particular manifestation is the topolog-

ical spin liquid (TSL) [29], a category including resonating valence-bond (RVB) states [30] and states hosting excitations with non-Abelian fractional quantum statistics, long sought in quantum information and topological quantum computation [31–33] (topological protection against decoherence). One experimental example of topological order is the fractional quantum Hall effect, where the excitations are usually Abelian [34]. The search for realistic TSL models gained momentum after the demonstration [30] of a Z_2 TSL ground state for the $S = 1/2$ kagome antiferromagnet. Recent progress has been due largely to advanced numerical methods, including extension of the quasi-1D density matrix renormalization group (DMRG) approach [30] to 2D TSLs [35] and the development of intrinsically high-dimensional techniques such as the projected entangled-pair states (PEPS) ansatz [36] and its extension to “simplex” lattice units [37]. PEPS have been used in TSLs for: (i) very efficient representation of the RVB state [38], (ii) classifying the topologically distinct ground states of the kagome antiferromagnet [39], and (iii) demonstrating a TSL in the antiferromagnetic J_1 - J_2 model on the square lattice [40]. Despite these recent breakthroughs, however, the fingerprints of topological order remain notoriously difficult to detect definitively, and any exactly solvable model with a TSL ground state [41] would be of enormous value.

In this Letter we solve exactly the Kumar model [25] on a *ring* and investigate: (i) spin-orbital entanglement, (ii) ground state degeneracy, (iii) nature of excitations, and (iv) scaling of the excitation gap with increasing system size. We show that, surprisingly, the properties of the Kumar model are determined by topology when the closing bond removes the total disorder in spins and generates spin-orbital entanglement in the ground state.

We consider the following model on a *ring* of length L with periodic boundary condition,

$$\mathcal{H} = \sum_{l=1}^L X_{l,l+1} (\tau_{l+1}^+ \tau_l^- + \tau_{l+1}^- \tau_l^+), \quad (1)$$

where $X_{l,l+1} = (1 + \vec{\sigma}_l \cdot \vec{\sigma}_{l+1})/2$ is a *spin transposition* operator on the bond $\langle l, l+1 \rangle$, i.e., $X_{l,l+1} \vec{\sigma}_l X_{l,l+1} = \vec{\sigma}_{l+1}$, where σ_l 's are spin Pauli matrices, and τ_l 's are orbital Pauli matrices. For an open chain [25], the spins and orbitals are decoupled by a unitary transformation,

$$\mathcal{U} = \prod_{l=1}^{L-1} \left[\frac{1 - \tau_{l+1}^z}{2} + \frac{1 + \tau_{l+1}^z}{2} \chi_{l+1,l} \right], \quad (2)$$

where $\chi_{l+1,l}$ is a *spin permutation* operator composed of the spin transpositions $X_{i,j}$:

$$\chi_{l+1,l} = X_{l+1,l} X_{l,l-1} \dots X_{3,2} X_{2,1}. \quad (3)$$

For a periodic chain, the same \mathcal{U} maps the model (1) to

$$\tilde{\mathcal{H}} = \mathcal{U}^\dagger \mathcal{H} \mathcal{U} = \left(\sum_{l=1}^{L-1} \tau_{l+1}^+ \tau_l^- + R_1^{(1)} R_1^{(2)} \tau_1^+ \tau_L^- \right) + \text{h.c.} \quad (4)$$

Here $R_p^{(1)}$ is a cyclic permutation of spins at sites $l = 1, \dots, N$ by p sites, $R_p^{(1)} \vec{\sigma}_l R_p^{(1)\dagger} = \vec{\sigma}_{l+p}$, and $R_p^{(2)}$ is the same permutation at sites $l = (N+1), \dots, L$. Thereby the ring separates into two parts of length N and $(L-N)$, with N being a good quantum number of ‘‘up’’ orbitals,

$$N = \frac{1}{2} \sum_{l=1}^L (1 + \tau_l^z). \quad (5)$$

For more details on the derivation of Eq. (4) see the Supplemental Material [42].

Unlike in an open chain, the spins are not fully integrated out but show up at the closing bond $\langle L, 1 \rangle$ of the Hamiltonian (4). The unitary operator $R_1^{(1)}$ has eigenvalues $e^{i\mathcal{K}_1}$ with a quasimomentum $\mathcal{K}_1 = 2\pi n_1/N$ and $n_1 = 0, \dots, N-1$. Similarly, for $R_1^{(2)}$ we get $\mathcal{K}_2 = 2\pi n_2/(L-N)$ and $n_2 = 0, \dots, L-N-1$. Thus the spin sector enters $\tilde{\mathcal{H}}$ as a single phase factor on the $\langle L, 1 \rangle$ bond,

$$\tilde{\mathcal{H}} = \sum_{l=1}^{L-1} \left(\tau_{l+1}^+ \tau_l^- + e^{i(\mathcal{K}_1 + \mathcal{K}_2)} \tau_L^+ \tau_1^- + \text{h.c.} \right). \quad (6)$$

It can be diagonalized by a Jordan-Wigner (JW) transformation, $\tau_l^z = 1 - 2n_l$, $\tau_l^+ = c_l \prod_{j<l} (1 - 2n_j)$, where c_l annihilates a JW fermion and $n_l = c_l^\dagger c_l$:

$$\tilde{\mathcal{H}} = \sum_{l=1}^{L-1} \left(c_{l+1}^\dagger c_l + e^{-2\pi i \Phi} c_l^\dagger c_L + \text{h.c.} \right) = 2 \sum_k c_k^\dagger c_k \cos k. \quad (7)$$

Here the phase $\Phi = n_1/N + n_2/(L-N) - (L-N-1)/2$ is twisting the boundary condition, $c_{L+1} = e^{2\pi i \Phi} c_1$, just like an Aharonov-Bohm magnetic flux Φ through the periodic ring. The schematic view of the spin-orbital decoupling is shown in Fig. 1. Note that correlated states are also found in the 1D XY \otimes XY spin-orbital model [43], but here their properties are more subtle, see below.

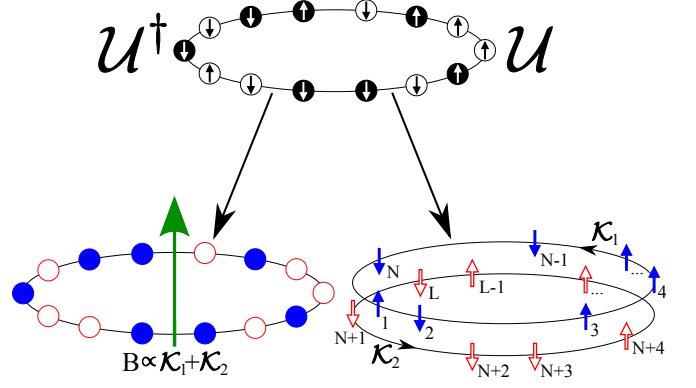


Figure 1. (color online) Artist’s view of the spin-orbital decoupling in the ring Eq. (1) caused by the transformation \mathcal{U} . The initial spin-orbital chain (top) splits into purely orbital (left) and spin (right) segments. The orbital part feels an external magnetic field \vec{B} perpendicular to the ring (arrow) produced by the spin flows \mathcal{K}_1 and \mathcal{K}_2 .

The quasimomenta in Eq. (7) are quantized as $k = 2\pi(m + \Phi)/L$, where $m = 0, \dots, (L-1)$. Assuming that L is even, \mathcal{H} is minimized by $N = L/2$ and

$$\mathcal{K} \equiv \mathcal{K}_1 + \mathcal{K}_2 = 0, \quad (8)$$

meaning that half of the orbitals are up, or the Fermi sea $|O\rangle$ is half-filled with the JW fermions. At the same time, there are two anticorrelated flows in the spin half-chains: when the first one has a quasimomentum \mathcal{K}_1 , the second one has the opposite quasimomentum $\mathcal{K}_2 = -\mathcal{K}_1$.

To see the action of the transformation back to the original basis more clearly, we represent the orbital Fermi sea in the τ^z -eigenbasis as $|O\rangle = \sum_{\vec{\alpha}} O_{\vec{\alpha}} |\vec{\alpha}\rangle$, where $\tau_l^z |\vec{\alpha}\rangle = \alpha_l |\vec{\alpha}\rangle$, which gives in the original basis,

$$\mathcal{U}|O\rangle = \sum_{\vec{\alpha}} O_{\vec{\alpha}} |\vec{\alpha}\rangle \mathcal{U}_{\vec{\alpha}}. \quad (9)$$

The orbital state $|\vec{\alpha}\rangle$ is not altered, but the spins are subject to a permutation $\mathcal{U}_{\vec{\alpha}}$ that maps the spins $\{N, \dots, 1\}$ to the successive N sites with orbitals ‘‘up’’ ($\alpha_l = 1$), and the spins $\{N+1, \dots, 2N\}$ to the remaining N successive sites with orbitals ‘‘down’’ ($\alpha_l = -1$). As the sequence of spins $\{1, \dots, N\}$ is *reversed* by the transformation, the spin-flow anticorrelation transforms into a correlation between the spin flow \mathcal{K}_1 on sites with orbitals up and the flow $\mathcal{K}_2 = \mathcal{K}_1$ on sites with orbitals down. The spin-orbital entanglement in the ground state wave functions can be depicted as in Fig. 2, where first the purely orbital Fermi sea wave function $|O\rangle$ is decomposed in the τ_i^z basis, and then the ‘‘up’’ and ‘‘down’’ components are dressed with equal spin flows $\{\mathcal{K}_1, \mathcal{K}_2\}$. This demonstrates the spin-orbital entanglement present in all the quasimomentum states which form the ground state.

Among the excited states one has to distinguish between the orbital excited states of the chain (7) for a

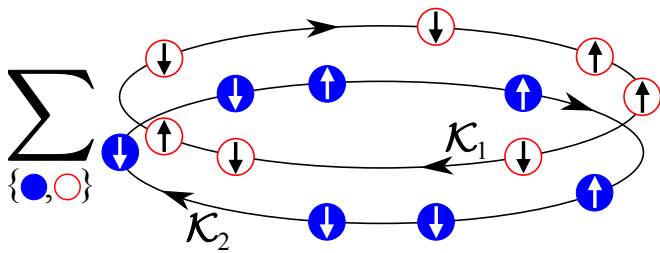


Figure 2. (color online) Schematic view of the ground state of the model (1). The system is divided into orbital "up" (empty circles) and orbital "down" (full circles) subsystems carrying the spin flows \mathcal{K}_1 and \mathcal{K}_2 . The flows are synchronized in this representation in each component: $\mathcal{K}_1 = \mathcal{K}_2$. Despite this nonlocal correlation, the local orientation of individual spins is (almost) random. Here the sum runs over all orbital configurations with the same number $N = L/2$ of "up" and "down" orbitals with amplitudes that are omitted here.

fixed \mathcal{K} , and the excitations with energy increased because of finite \mathcal{K} , or asynchronized flows $\mathcal{K}_1, \mathcal{K}_2$ in Fig. 2. The latter are of interest here as they arise from the degenerate manifold of 2^L ground states of an open chain and gain finite dispersion only due to the change of topology caused by the closing bond — they can be regarded as *topological excitations*. The energy of such excitations depends on total quasimomentum $\mathcal{K} = 2\pi n/N \neq 0$ that enters the orbital Hamiltonian (7). Thus every \mathcal{K} -excited state is related with a different orbital ground state where all the quasimomenta k from the Fermi sea gain a shift of $\delta k = \mathcal{K}/L$ with respect to the global ground state. This shows both non-local and entangled nature of the topological excitations which change the global spin flows and shift the orbital Fermi sea at the same time. The multiplet structure of the \mathcal{K} -excited states is such that the first excited state has $n = \pm 1$ corresponding to $\mathcal{K} = \pm 2\pi/N$. The second excited state is obtained with $n = \pm 2$ and so on, see Fig. 3 for classification of the excitations. Their dispersion is quadratic in n for $|n| \ll L/2$ and large L ,

$$\mathcal{E}_n = -\frac{2L}{\pi} + 16\pi \frac{n^2}{L^3}. \quad (10)$$

The energy gap between the orbital ground states for $n = 0$ and $n = \pm 1$ for nanoscopic systems. It scales as L^{-3} , while the orbital gap gradually closes with increasing system size, and for a given n decays as L^{-1} .

We now solve the problem of the ground state degeneracy for the spin-orbital $SU(2) \otimes XY$ ring Eq. (1). An eigenstate of $R_1^{(1)}$ with eigenvalue $e^{i\mathcal{K}_1}$ can be generated from the m_1 -th basis state $|m_1\rangle$ of spins $1, \dots, N$ as

$$|\mathcal{K}_1, m_1\rangle = \frac{1}{\sqrt{N}} \sum_{p=0}^{N-1} e^{-i\mathcal{K}_1 p} R_p^{(1)} |m_1\rangle. \quad (11)$$

Analogously, one gets the $e^{i\mathcal{K}_2}$ -eigenstate for spins labeled as $(N+1), \dots, 2N$. Note that the basis states $|m_i\rangle$

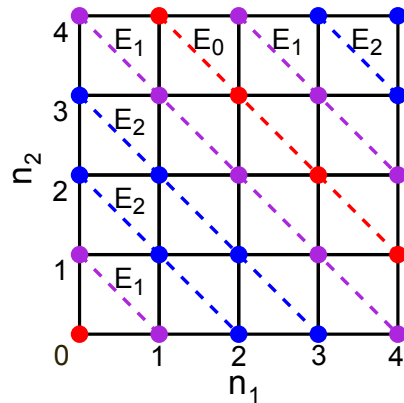


Figure 3. (color online) Energies of the lowest topological excitations for $L = 10$ and $N = L/2 = 5$ in the periodic (n_1, n_2) reciprocal plane. Dots connected by dashed lines represent different energies E_m — the lines of constant $n = 0, 1, 2$, where $n = n_1 + n_2$, are shown as a guide for the eye.

that are periodic under cyclic permutations $R_p^{(i)}$ with $p < N$ can generate $\mathcal{K}_i = 2\pi n/p$, with $n = 0, \dots, (p-1)$ only. For instance, the ferromagnetic (FM) state can generate only $\mathcal{K}_i = 0$ and the anti-FM one $\mathcal{K}_i = 0, \pi$. In case of a prime N , the only periodic states are the two FM states. Thus there are $\mathcal{N} = (2^N - 2)/N$ quasimomentum-degenerate eigenstates when $\mathcal{K}_i \neq 0$, and their number is $\mathcal{N} + 2$ for $\mathcal{K}_i = 0$. The total ground state degeneracy is

$$\mathcal{D} = (N-1)\mathcal{N}^2 + (\mathcal{N}+2)^2. \quad (12)$$

For a large system size one finds $\mathcal{D} \approx 2^{L+1}/L$ as compared to $\mathcal{D}_0 = 2^L$ for an open chain. Thus, the degeneracy is drastically reduced by the topological correlations introduced by the periodic boundary conditions.

To understand the structure of the degenerate ground state, we analyze now the spin and orbital part. Due to the degeneracy, the zero temperature state is a mixed state. In the new basis, its density matrix is a product $\tilde{\rho} = |O\rangle \langle O| \rho_S$, where the spin state is

$$\rho_S = \frac{1}{\mathcal{D}} \sum_{\mathcal{K}} \sum_{m_1 m_2} |-\mathcal{K}, m_1\rangle \langle -\mathcal{K}, m_1| |\mathcal{K}, m_2\rangle \langle \mathcal{K}, m_2|. \quad (13)$$

Back in the physical representation, the product state $\rho = \mathcal{U} \tilde{\rho} \mathcal{U}^\dagger$ becomes spin-orbital entangled by the inverse transformation (9). In the orbital sector, this transformation is a pure decoherence in the pointer basis of τ_1^z [44]. In this basis the orbital state $|\vec{\alpha}\rangle$ does not change, but the spins are subject to a transformation $\mathcal{U}_{\vec{\alpha}}$ that depends on the orbital state:

$$\rho = \frac{1}{\mathcal{D}} \sum_{\vec{\alpha}, \vec{\beta}} O_{\vec{\alpha}} O_{\vec{\beta}}^* \sum_{\mathcal{K}, m_1, m_2} |\vec{\alpha}\rangle \mathcal{U}_{\vec{\alpha}} |-\mathcal{K}, m_1\rangle |\mathcal{K}, m_2\rangle \langle -\mathcal{K}, m_1| \langle \mathcal{K}, m_2| \mathcal{U}_{\vec{\beta}}^\dagger |\vec{\beta}\rangle. \quad (14)$$

Thus the orbital state $|\vec{\alpha}\rangle$ becomes entangled with spin states $\mathcal{U}_{\vec{\alpha}} |-\mathcal{K}, m_1\rangle |\mathcal{K}, m_2\rangle$, and with a flow \mathcal{K} at sites

$\alpha_l = 1$ and another flow \mathcal{K} at sites $\alpha_l = -1$. The entanglement has decoherence effect,

$$\rho_O = \text{Tr}_S \rho = \sum_{\vec{\alpha}, \vec{\beta}} |\vec{\alpha}\rangle O_{\vec{\alpha}} D_{\vec{\alpha}, \vec{\beta}} O_{\vec{\beta}}^* |\vec{\beta}\rangle, \quad (15)$$

comparing with the pure orbital state before the inverse \mathcal{U} -transformation, $|O\rangle\langle O| = \sum_{\vec{\alpha}, \vec{\beta}} |\vec{\alpha}\rangle O_{\vec{\alpha}} O_{\vec{\beta}}^* \langle \vec{\beta}|$. The coherences are suppressed by the decoherence factors,

$$D_{\vec{\alpha}, \vec{\beta}} = \text{Tr}_S \mathcal{U}_{\vec{\alpha}} \rho_S \mathcal{U}_{\vec{\beta}}^\dagger, \quad (16)$$

but the probabilities $O_{\vec{\alpha}} O_{\vec{\alpha}}^*$ are invariant, $D_{\vec{\alpha}, \vec{\alpha}} = 1$. Since ρ_S in (13) is a diagonal ensemble of spin ground states $|S\rangle\langle S|$, $D_{\vec{\alpha}, \vec{\beta}}$ measures how much orthogonal the states $\mathcal{U}_{\vec{\alpha}}|S\rangle$ and $\mathcal{U}_{\vec{\beta}}|S\rangle$ are or, equivalently, how much entangled with spins the orbital states $|\vec{\alpha}\rangle$ and $|\vec{\beta}\rangle$ become for a typical $|S\rangle$.

Since the τ^z -basis is the basis of JW fermionic occupation numbers, the decoherence is localizing the JW fermions that were originally delocalized in the Fermi sea $|O\rangle$. To get an idea how tight the localization is, we can consider an open chain where the closing bond $(L, 1)$ is missing and, consequently, the spin state is arbitrary, $\rho_S \propto 1$. One finds a compact formula,

$$\log_2 D_{\vec{\alpha}, \vec{\beta}} = -L + \sum_{p=1}^L \delta_{0, \sum_{i=1}^p (\alpha_i - \beta_i)}. \quad (17)$$

An illustrative example are states $\vec{\alpha}$ and $\vec{\beta}$ which differ at only two sites $\{i, j\}$. Then $D_{\vec{\alpha}, \vec{\beta}} = 2^{-|i-j|}$ is localized exponentially on the scale of $(\ln 2)^{-1} = 1.44$ sites.

The short localization length suggests that Eq. (17) is a good approximation in the periodic case as well. Indeed, in case of prime N one finds that

$$D_{\vec{\alpha}, \vec{\beta}} = \frac{1}{ND} \sum_{p=0}^{N-1} \text{Tr}_S \mathcal{U}_{\vec{\beta}}^\dagger \mathcal{U}_{\vec{\alpha}} R_{-p}^{(1)} R_{-p}^{(2)} = \frac{1}{ND} \sum_{p=0}^{N-1} 2^{c_p}. \quad (18)$$

Here c_p is a number of cycles in a cyclic decomposition of the permutation $\mathcal{U}_{\vec{\beta}}^\dagger \mathcal{U}_{\vec{\alpha}} R_{-p}^{(1)} R_{-p}^{(2)}$. Again, for $\vec{\alpha}$ and $\vec{\beta}$ that differ only at sites $\{i, j\}$ without loss of generality we set $i=1$, $j=1+R$, with $1 \leq R \leq N$, and $\alpha_1 = \beta_{1+R} = 1$, $\alpha_{1+R} = \beta_1 = -1$, and introduce integer sums,

$$a_{\pm} = \frac{1}{2} \sum_{l=2}^R (1 \pm \alpha_l), \quad b_{\pm} = \frac{1}{2} \sum_{l=R+2}^{2N} (1 \pm \alpha_l). \quad (19)$$

They can be decomposed as $a_{\pm} = C_{\pm}(p-1) + A_{\pm}$ and $b_{\pm} = (p-1) + D_{\pm}p + B_{\pm}$, where C_{\pm}, D_{\pm} are integers and A_{\pm}, B_{\pm} are integer remainders: $0 \leq A_{\pm} < (p-1)$ and $0 \leq B_{\pm} < p$. The numbers of cycles c_p can now be written in a more compact form. In particular, $c_0 = 2N - R$, $c_1 = R$, and for $p \geq 2$ we obtain

$$c_{p \geq 2} = \mathcal{C} [R_{p, B_+} R_{p-1, A_+}] + \mathcal{C} [R_{p, B_-} R_{p-1, A_-}] - 1. \quad (20)$$

Here R_{p, B_+} is a cyclic permutation of a p -element list by B_+ sites, and R_{p-1, A_+} refers to the first $(p-1)$ elements of this list. The function \mathcal{C} counts the number of cycles. From Eq. (20) we can estimate that $c_{p \geq 2} \leq 2p-1$. Since $c_{N-p} = c_p$, it follows $c_{p \geq 2} \leq 2(N-1)/2-1 = N-2$. For large N the sum (18) is dominated by the $p=0$ term,

$$D_{\vec{\alpha}, \vec{\beta}} \approx \frac{1}{ND} [2^{2N-R} + 2 \times 2^R + \mathcal{O}(N2^N)] \approx 2^{-R}, \quad (21)$$

with the same localization length as in the open chain. This result illustrates the general smallness of decoherence factors corroborating the picture of non-trivial spin-orbital entanglement represented in Fig. 2. For more details see the Supplemental Material [42].

Summarizing, we have shown rigorously that closing the spin-orbital chain with $\text{SU}(2) \otimes \text{XY}$ exchange Eq. (1) causes surprising changes in the spin part of the lowest-lying eigenstates. Spins are not decoupled from the orbitals, as it happens in the open chain, but instead the spin states associated with the orbital ground state are structured in a multiplet labeled by their quasimomentum. We have found that this change of the exact eigenstates: (i) reduces the degeneracy of the ground state and, more importantly, (ii) triggers nontrivial topological order with spin-orbital entanglement.

Similar entanglement concerns also the excited states — spin excitations have definite quasimomenta on sites where the orbitals are polarized up and on those polarized down, and the total quasimomentum is a good topological quantum number. These topological excitations have a dispersion quadratic in the quasimomentum and a nontrivial gap scaling exponent: $\Delta \propto L^{-\eta}$ with $\eta = 3$. The orbital decoherence caused by the inverse \mathcal{U} -transformation, that entangles spins with orbitals, localizes the orbital quasiparticles on a very short length scale, both for periodic and open chains.

We thank particularly warmly Bruce Normand for valuable advice, and Giniyat Khaliullin and Krzysztof Wohlfeld for insightful discussions. We acknowledge financial support by the Polish National Science Center (NCN) under Projects No. 2012/04/A/ST3/00331 (W.B. and A.M.O) and 2011/01/B/ST3/00512 (J.D.).

SUPPLEMENTAL MATERIAL

In the first Section of this Supplemental Material we present the derivation of the unitary transformation on the closing bond in the spin-orbital model introduced by Kumar [B. Kumar, Phys. Rev. B **87**, 195105 (2013)], see Eq. (1) of the Letter. In the second Section we show the technical details which justify our analysis of the structure of the correlated states which form the degenerate ground state of the closed $SU(2) \otimes XY$ spin-orbital ring.

The closing bond in the $SU(2) \otimes XY$ Hamiltonian

Here we derive the result of the unitary transformation

$$\begin{aligned} \mathcal{U} &= \prod_{l=1}^{L-1} \left[\frac{1 - \tau_{l+1}^z}{2} + \frac{1 + \tau_{l+1}^z}{2} \chi_{l+1,l} \right] \\ &\equiv \prod_{l=1}^{L-1} [P_{l+1}^- + P_{l+1}^+ \chi_{l+1,l}], \end{aligned} \quad (22)$$

on the periodic Kumar Hamiltonian

$$\mathcal{H} = \sum_{l=1}^L X_{l,l+1} (\tau_{l+1}^+ \tau_l^- + \tau_{l+1}^- \tau_l^+). \quad (23)$$

We focus on the closing bond $\langle L, 1 \rangle$ in Eq. (2). It is enough to consider the transformation,

$$\begin{aligned} \mathcal{U}^\dagger X_{L,1} \tau_1^+ \tau_L^- \mathcal{U} &= \\ &\prod_{l=L-1}^1 [P_{l+1}^- + P_{l+1}^+ \chi_{l+1,l}^\dagger] \times \\ &X_{L,1} \tau_1^+ \tau_L^- \prod_{l'=1}^{L-1} [P_{l'+1}^- + P_{l'+1}^+ \chi_{l'+1,l'}] = \\ &\prod_{l=L-1}^1 [P_{l+1}^- + P_{l+1}^+ \chi_{l+1,l}^\dagger] \times \\ &X_{L,P_1^+} \tau_1^+ \tau_L^- \prod_{l'=1}^{L-1} [P_{l'+1}^- + P_{l'+1}^+ \chi_{l'+1,l'}] = \\ &\prod_{l=L-1}^2 [P_{l+1}^- + P_{l+1}^+ \chi_{l+1,l}^\dagger] \times \\ &X_{L,P_1^+ P_2^+} \tau_1^+ \tau_L^- \prod_{l'=2}^{L-1} [P_{l'+1}^- + P_{l'+1}^+ \chi_{l'+1,l'}] = \\ &\left[P_L^- + P_L^+ \chi_{L,L-1}^\dagger \right] \times \\ &X_{L,\sum_{l=1}^{L-1} P_l^+} \tau_1^+ \tau_L^- [P_L^- + P_L^+ \chi_{L,L-1}]. \end{aligned} \quad (24)$$

After further transformations one finds that

$$\begin{aligned} \mathcal{U}^\dagger X_{L,1} \tau_1^+ \tau_L^- \mathcal{U} &= \\ X_{L,\sum_{l=1}^{L-1} P_l^+} \tau_1^+ \tau_L^- \chi_{L,L-1} &= \\ X_{L,\sum_{l=1}^L P_l^+} \tau_1^+ \tau_L^- \chi_{L,L-1} &= \\ X_{L,N} \chi_{L,L-1} \tau_1^+ \tau_L^- &= \\ X_{L,N} X_{L,L-1} \dots X_{2,1} \tau_1^+ \tau_L^- &. \end{aligned} \quad (25)$$

The operator $R = X_{L,N} X_{L,L-1} \dots X_{2,1}$ is a spin permutation:

$$\begin{aligned} R \vec{\sigma}_1 R^\dagger &= \vec{\sigma}_N, \quad R \vec{\sigma}_2 R^\dagger = \vec{\sigma}_1, \dots, \quad R \vec{\sigma}_N R^\dagger = \vec{\sigma}_{N-1}, \\ R \vec{\sigma}_{N+1} R^\dagger &= \vec{\sigma}_L, \quad R \vec{\sigma}_{N+2} R^\dagger = \vec{\sigma}_{N+1}, \dots, \quad R \vec{\sigma}_L R^\dagger = \vec{\sigma}_{L-1}, \end{aligned}$$

i.e., it is a cyclic permutation of spins $1, \dots, N$ by one site, and the same permutation of spins $(N+1), \dots, L$. In other words, the permutation R factorizes into two cycles, $R = R_1^{(1)} R_1^{(2)}$, where

$$\begin{aligned} R_1^{(1)} &= X_{N,N-1} \dots X_{2,1}, \\ R_1^{(2)} &= X_{L,L-1} \dots X_{N+2,N+1}. \end{aligned} \quad (26)$$

Finally, the closing bond becomes

$$\mathcal{U}^\dagger X_{L,1} \tau_1^+ \tau_L^- \mathcal{U} + \text{h.c.} = R_1^{(1)} R_1^{(2)} \tau_1^+ \tau_L^- + \text{h.c.}, \quad (27)$$

which justifies Eq. (4) of the Letter.

Permutation cycles and decoherence factors

We need a more efficient formula for the number of cycles c_p in the cycle decomposition of the permutation $\mathcal{U}_\beta^\dagger \mathcal{U}_\alpha R_{-p}^{(1)} R_{-p}^{(2)}$:

$$c_p = \mathcal{C} \left(\mathcal{U}_\beta^\dagger \mathcal{U}_\alpha R_{-p}^{(1)} R_{-p}^{(2)} \right). \quad (28)$$

Notice that the number of cycles is invariant under cyclic permutations:

$$\mathcal{C} \left(\mathcal{U}_\beta^\dagger \mathcal{U}_\alpha R_{-p}^{(1)} R_{-p}^{(2)} \right) = \mathcal{C} \left(\mathcal{U}_\alpha R_{-p}^{(1)} R_{-p}^{(2)} \mathcal{U}_\beta^\dagger \right) = \dots \quad (29)$$

just like the trace operation.

The transformation \mathcal{U}_α maps the spins $N, \dots, 1$ to the spins at the N successive sites with orbitals up, where $\alpha_l = 1$, and the spins $N+1, \dots, 2N$ to the spins at the remaining N successive sites with orbitals down, where $\alpha_l = -1$. It is convenient to make a decomposition:

$$\mathcal{U}_\alpha = \mathcal{V}_\alpha \mathcal{P}^{(1)}. \quad (30)$$

Here $\mathcal{P}^{(1)}$ is a parity operation that maps the spins $1, \dots, N$ to the spins $N, \dots, 1$, i.e., inverts the order of spins $1, \dots, N$. \mathcal{V}_α maps the spins $1, \dots, N$ to the spins at the N successive sites with orbitals up, where $\alpha_l = 1$ and the spins $N+1, \dots, 2N$ to the remaining N successive sites

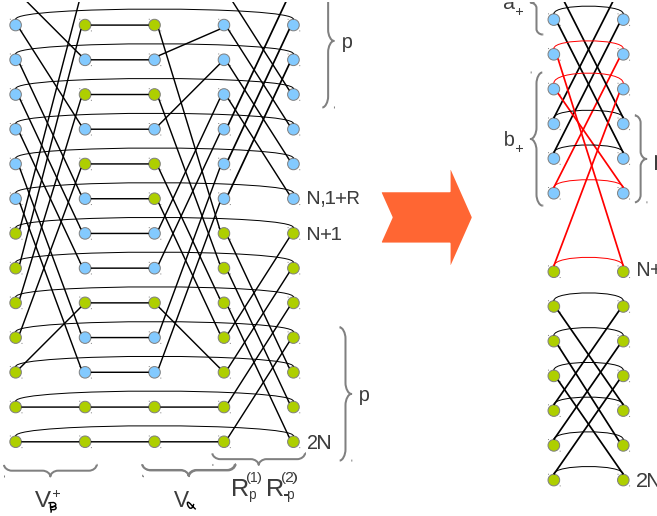


Figure 4. In A, graphic representation of $\text{Tr} \left[\mathcal{V}_\beta^\dagger \mathcal{V}_\alpha R_p^{(1)} R_{-p}^{(2)} \right]$. Here each circle represents a spin. The blue circles represent spins at the sites $1, \dots, N$ that are mapped by \mathcal{V}_α (or \mathcal{V}_β) to the sites with orbitals up, where $\alpha_l = 1$ (or $\beta_l = 1$). The green ones represent spins $(N+1), \dots, 2N$ that are mapped to the sites with orbitals down. The circles/spins are connected by lines that represent actions of the permutations on each spin. The connecting lines make c_p closed loops. Each loop contributes a factor of 2 to the trace represented by graph A. Here we chose $N = 7$, $R = 6$, $p = 4$, $a_+ = 2$, $b_+ = 4$, $a_- = 3$, $b_- = 3$ for illustration, but the argument can be generalized to arbitrary values of the parameters. In B, after the three middle spin columns in graph A are eliminated, we obtain graph B with the same number of loops. This graph can be divided into the top half (spins $1, \dots, N$ /blue circles) and the bottom one (spins $N+1, \dots, 2N$ /green circles). Notice that there is exactly one closed loop (marked red) that is common to the two halves. In the next Fig. 5 we continue with the top half, the analysis of the bottom one follows the same lines, but with $\{a_+, b_+\}$ replaced by $\{a_-, b_-\}$.

with orbitals down, where $\alpha_l = -1$. Using the cyclic invariance and this decomposition we obtain

$$\begin{aligned} c_p &= \mathcal{C} \left(\mathcal{V}_\beta^\dagger \mathcal{V}_\alpha \mathcal{P}^{(1)} R_{-p}^{(1)} R_{-p}^{(2)} \mathcal{P}^{(1)} \right) \\ &= \mathcal{C} \left(\mathcal{V}_\beta^\dagger \mathcal{V}_\alpha \mathcal{P}^{(1)} R_{-p}^{(1)} \mathcal{P}^{(1)} R_{-p}^{(2)} \right) \\ &= \mathcal{C} \left(\mathcal{V}_\beta^\dagger \mathcal{V}_\alpha R_p^{(1)} R_{-p}^{(2)} \right). \end{aligned} \quad (31)$$

The trace of the permutation $\mathcal{V}_\beta^\dagger \mathcal{V}_\alpha R_p^{(1)} R_{-p}^{(2)}$ is graphically represented in Fig. 4A. The number of cycles c_p is the number of closed loops in this diagram.

Figures 4 and 5 show a step-by-step reduction of the diagram 4A to a more and more compact form. The intermediate graph 4B can be split into the top and bottom halves [spins $1, \dots, N$ and $(N+1), \dots, 2N$ respectively] that have one loop in common. In the following Fig. 5A, the common loop is included to the top half.

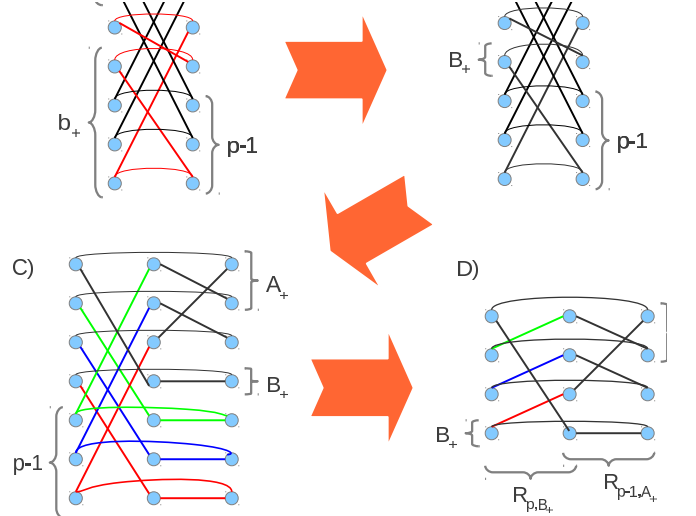


Figure 5. In A, the top half of the graph in Fig. 4B, but with the common loop connecting the top and bottom halves contracted to the top half. In B, the same as in A, but after application of the decompositions $a_+ = C_+(p-1) + A_+$ and $b_+ = (p-1) + D_+p + B_+$ with integer C_+, A_+, D_+, B_+ and $|A_+| < p-1, |B_+| < p$. Here $C_+ = D_+ = 0$ but in general, even when C_+ or D_+ are non-zero, the graph can be contracted to this form. In C, graph B is transformed into a cyclic rotation of the first $A_+ + 1$ spins followed by a cyclic rotation of all $A_+ + B_+ + p$ spins by $-(p-1)$ elements. Notice the $p-1$ chains (marked green, blue, and red) that can be contracted to the $p-1$ single segments in graph D (marked green, blue, and red respectively). In D, the final graph with the same number of closed loops as the top half of the graph in Fig. 4B including the common loop. Here a cyclic rotation of the first $p-1$ spins by A_+ sites is followed by a cyclic rotation of all p spins by B_+ sites.

Finally, the number of cycles (loops) in the top half, enlarged with the common loop, can be read from the graph 5D as

$$\mathcal{C} [R_{p,B_+} R_{p-1,A_+}]. \quad (32)$$

Here R_{p,B_+} is a cyclic permutation of a p -element list by B_+ sites, and R_{p-1,A_+} refers to the first $(p-1)$ elements of that list. In a similar way, the number of loops in the bottom half of the graph 4B, enlarged with the common loop, can be obtained as

$$\mathcal{C} [R_{p,B_-} R_{p-1,A_-}]. \quad (33)$$

When the two halves are put together again their number of cycles becomes a sum,

$$c_p = \mathcal{C} [R_{p,B_+} R_{p-1,A_+}] + \mathcal{C} [R_{p,B_-} R_{p-1,A_-}] - 1, \quad (34)$$

with the -1 to correct for the double counting of the loop common to both halves.

-
- [1] Y. Tokura and N. Nagaosa, *Science* **288**, 462 (2000).
- [2] J. van den Brink, Z. Nussinov, and A.M. Oleś, in: *Introduction to Frustrated Magnetism: Materials, Experiments, Theory*, edited by C. Lacroix, P. Mendels, and F. Mila (Springer, New York, 2011).
- [3] G. Khaliullin, *Prog. Theor. Phys. Suppl.* **160**, 155 (2005).
- [4] A.M. Oleś, G. Khaliullin, P. Horsch, and L.F. Feiner, *Phys. Rev. B* **72**, 214431 (2005).
- [5] A.M. Oleś, *J. Phys.: Condens. Matter* **24**, 313201 (2012).
- [6] K.I. Kugel and D.I. Khomskii, *Sov. Phys. Usp.* **25**, 231 (1982).
- [7] L.F. Feiner, A.M. Oleś, and J. Zaanen, *Phys. Rev. Lett.* **78**, 2799 (1997); *J. Phys.: Condens. Matter* **10**, L555 (1998); G. Khaliullin and V. Oudovenko, *Phys. Rev. B* **56**, R14243 (1997).
- [8] W. Brzezicki, J. Dziarmaga, and A.M. Oleś, *Phys. Rev. Lett.* **109**, 237201 (2012); *Phys. Rev. B* **87**, 064407 (2013); W. Brzezicki and A.M. Oleś, *ibid.* **83**, 214408 (2011).
- [9] Fa Wang and A. Vishwanath, *Phys. Rev. B* **80**, 064413 (2009); M. Lajkó and K. Penc, *ibid.* **87**, 224428 (2013); P. Corboz, M. Lajkó, A.M. Läuchli, K. Penc, and F. Mila, *Phys. Rev. X* **2**, 041013 (2012).
- [10] B. Normand and A.M. Oleś, *Phys. Rev. B* **78**, 094427 (2008); B. Normand, *ibid.* **83**, 064413 (2011); J. Chaloupka and A.M. Oleś, *ibid.* **83**, 094406 (2011).
- [11] K. Wohlfeld, M. Daghofer, S. Nishimoto, G. Khaliullin, and J. van den Brink, *Phys. Rev. Lett.* **107**, 147201 (2011); K. Wohlfeld, S. Nishimoto, M.W. Haverkort, and J. van den Brink, arXiv:1307.6180 (2013).
- [12] J. Schlappa *et al.*, *Nature (London)* **485**, 82 (2012).
- [13] R. Lundgren, V. Chua, and G.A. Fiete, *Phys. Rev. B* **86**, 224422 (2012).
- [14] C. Itoi, S. Qin, and I. Affleck, *Phys. Rev. B* **61**, 6747 (2000).
- [15] J. van den Brink, W. Stekelenburg, D.I. Khomskii, G.A. Sawatzky, and K.I. Kugel, *Phys. Rev. B* **58**, 10276 (1998); J. Sirker, *ibid.* **69**, 104428 (2004).
- [16] Y. Chen, Z.D. Wang, Y.Q. Li, and F.C. Zhang, *Phys. Rev. B* **75**, 195113 (2007).
- [17] W.-L. You, A.M. Oleś, and P. Horsch, *Phys. Rev. B* **86**, 094412 (2012).
- [18] G. Khaliullin, P. Horsch, and A.M. Oleś, *Phys. Rev. Lett.* **86**, 3879 (2001); C. Ulrich, G. Khaliullin, J. Sirker, M. Reehuis, M. Ohl, S. Miyasaka, Y. Tokura, and B. Keimer, *ibid.* **91**, 257202 (2003); P. Horsch, G. Khaliullin, and A.M. Oleś, *ibid.* **91**, 257203 (2003); A.M. Oleś, P. Horsch, L.F. Feiner, and G. Khaliullin, *ibid.* **96**, 147205 (2006); P. Horsch, A.M. Oleś, L.F. Feiner, and G. Khaliullin, *ibid.* **100**, 167205 (2008); J. Sirker, A. Herzog, A.M. Oleś, and P. Horsch, *ibid.* **101**, 157204 (2008).
- [19] Y. Q. Li, M. Ma, D.N. Shi, and F.C. Zhang, *Phys. Rev. Lett.* **81**, 3527 (1998); B. Frischmuth, F. Mila, and M. Troyer, *ibid.* **82**, 835 (1999); P. Azaria, A.O. Gogolin, P. Lecheminant, and A.A. Nersisyan, *ibid.* **83**, 624 (1999).
- [20] A.M. Oleś, P. Horsch, and G. Khaliullin, *Phys. Stat. Solidi B* **244**, 2378 (2007).
- [21] This state is similar to the Majumdar-Ghosh state in a 1D J_1 - J_2 spin chain, see C.K. Majumdar and D.K. Ghosh, *J. Math. Phys.* **10**, 1388 (1969).
- [22] J. van den Brink, *New J. Phys.* **6**, 201 (2004); J. van den Brink, P. Horsch, F. Mack, and A.M. Oleś, *Phys. Rev. B* **59**, 6795 (1999); L. Cincio, J. Dziarmaga, and A.M. Oleś, *ibid.* **82**, 104416 (2010); A. van Rynbach, S. Todo, and S. Trebst, *Phys. Rev. Lett.* **105**, 146402 (2010).
- [23] S.K. Pati and R.R.P. Singh, *Phys. Rev. B* **61**, 5868 (2000).
- [24] A. Herzog, P. Horsch, A.M. Oleś, and J. Sirker, *Phys. Rev. B* **83**, 245130 (2011).
- [25] B. Kumar, *Phys. Rev. B* **87**, 195105 (2013).
- [26] G. Misguich, in: *Introduction to Frustrated Magnetism: Materials, Experiments, Theory*, edited by C. Lacroix, P. Mendels, and F. Mila (Springer, New York, 2011).
- [27] Leon Balents, *Nature (London)* **464**, 199 (2010).
- [28] Bruce Normand, *Cont. Phys.* **50**, 533 (2009).
- [29] Xiao-Gang Wen, *Phys. Rev. B* **65**, 165113 (2002).
- [30] S. Yan, D.A. Huse, and S.R. White, *Science* **332**, 1173 (2011); S. Depenbrock, I.P. McCulloch, and U. Schollwöck, *Phys. Rev. Lett.* **109**, 067201 (2012).
- [31] A. Kitaev and C. Laumann, in: *Exact Methods in Low-Dimensional Physics and Quantum Computing: Lecture Notes of the Les Houches Summer School Vol. 89*, ed. D. Serban, J. Jacobsen, L. Cugliandolo, S. Ouvry, and V. Pasquier (Oxford University Press, 2011); arXiv:0904.2771.
- [32] B. Douçot, M.V. Feigel'man, L.B. Ioffe, and A.S. Ioselevich, *Phys. Rev. B* **71**, 024505 (2005).
- [33] F. Trouselet, A.M. Oleś, and P. Horsch, *Europhys. Lett.* **91**, 40005 (2010); *Phys. Rev. B* **86**, 134412 (2012).
- [34] B.A. Bernevig and S.-C. Zhang, *Phys. Rev. Lett.* **96**, 106802 (2006).
- [35] L. Cincio and G. Vidal, *Phys. Rev. Lett.* **110**, 067208 (2013).
- [36] F. Verstraete and J.I. Cirac, arXiv:cond-mat/0407066v1 (2004).
- [37] Z.Y. Xie, J. Chen, J.F. Yu, X. Kong, B. Normand, and T. Xiang, arXiv:1307.5696 (2013); Z. Nussinov and B. Normand, arXiv:1308.3186 (2013).
- [38] D. Poilblanc, N. Schuch, D. Pérez-García, and J.I. Cirac, *Phys. Rev. B* **86**, 014404 (2012); N. Schuch, D. Poilblanc, J.I. Cirac, and D. Pérez-García, *ibid.* **86**, 115108 (2012).
- [39] D. Poilblanc and N. Schuch, *Phys. Rev. B* **87**, 140407(R) (2013).
- [40] L. Wang, D. Poilblanc, Z.-C. Gu, X.-G. Wen, and F. Verstraete, *Phys. Rev. Lett.* **111**, 037202 (2013).
- [41] A. Kitaev, *Annals of Physics* **321**, 2 (2006); G. Baskaran, S. Mandal, and R. Shankar, *Phys. Rev. Lett.* **98**, 247201 (2007); S.R. Hassan, P.V. Sriluckshmy, S.K. Goyal, R. Shankar, and D. Sénéchal, *ibid.* **110**, 037201 (2013).
- [42] See the Supplemental Material at <http://link.aps.org/>... for more technical details.
- [43] F. Mila, B. Frischmuth, A. Deppeler, and M. Troyer, *Phys. Rev. Lett.* **82**, 3697 (1999).
- [44] W.H. Żurek, *Phys. Rev. D* **24**, 1516 (1981).